Catalysis Today xxx (xxxx) xxx

Contents lists available at ScienceDirect

Catalysis Today

journal homepage: www.elsevier.com/locate/cattod

Parametric sensitivity analysis of the transient adsorption-diffusion models for hydrocarbon transport in microporous materials

Vladyslav Shostak [a], Evgeniy Redekop [a,*], Unni Olsbye [a]

[a] Department of Chemistry, University of Oslo, P.O. Box 1033, Blindern, N-0315 Oslo, Norway

A B S T R A C T

The complex nature of hydrocarbon transport in microporous materials offers unique challenges for the description of transient kinetic data in catalysis by e.g. acidic zeolites and zeotypes. Currently, very few models in the literature capture such phenomena as surface barriers or hindered microporous diffusion - processes that are known to impact gas transport during the kinetic studies of zeolite catalyzed reactions. In this work we provide extended models that reflect the aforementioned phenomena during pulse-response experiments in the Temporal Analysis of Products (TAP) reactor. Systematic studies of models' parametric sensitivity are presented to assist the design of future experiments. Numerical simulations are used to investigate how thermodynamic adsorption properties of realistic zeolites can affect the pulse-response shapes. For certain combination adsorption/diffusion parameters, microporous diffusion is shown to result in a characteristic bend in the mean residence time temperature dependency, which can be used as a fingerprint in model discrimination.

1. Introduction

Diffusion and reactions of hydrocarbons in zeolites and zeotypes remain one of the most challenging topics in Transient Kinetics as well as in other fields of natural and mathematical sciences [1–3]. Providing deeper understanding of mass-transport in zeolite catalysts is particularly important for gaining insights into and controlling the kinetics of catalytic reactions of many crucial industrial chemical processes. Transient kinetic techniques like Temporal Analysis of Products (TAP) can provide data on intrinsic kinetic properties which can, in principle, be quantitatively compared to microscopic measurements on model materials and/or ab initio studies. Unlike most microscopic methods of diffusion characterization, TAP experiments can be used to investigate pore diffusion simultaneously with chemical reactions. Furthermore, typical TAP Reactor Systems allow exposure of catalytic samples to more realistic reaction conditions under ambient pressure flow of reactants, followed by rapid and reproducible evacuation to the well-defined regime of Knudsen diffusion, where the impact of the flow pretreatment on the intrinsic kinetic and diffusion properties of the materials can be probed [4–6]. However, transient experiments are also impacted by, generally, multi-scale transport phenomena ranging from diffusion within individual crystallites to the reactor-scale fluid transport. The kinetic resolution of transient data is determined by how soundly these transport phenomena are reflected in mathematical models that are employed to estimate the intrinsic kinetic parameters from experimental measurements. Kinetics, after all, is only as accurate as the standard transport process used to measure it. Thus, systematic quantification of diffusion in zeolites can sharpen the fundamental understanding of reaction kinetics and, ultimately, help improve large-scale zeolite-catalyzed processes in industry.

The main challenge in investigating gas transport in zeolites is the manifold of simultaneously occurring processes. Several diffusion mechanisms can co-exist, including most common modes of diffusion (Knudsen, surface hopping, single-file) and other major or minor case-specific interactions [7]. Microscopic studies elucidated that a prevalent mechanism is often determined by the ratio between the sizes of the guest molecules and the host channels, channel shape, crystal shape and size, strength and frequency of interactions between guests and either internal and/or external active sites [8–10]. In macroscopic transport studies on technologically-relevant samples, diffusivity measurements are also influenced by phenomena occurring at the outer rim of zeolite crystallites. Observed hindrance at the zeolite outer shell is typically described as a "surface barrier". The origin of surface barriers is still unclear and proposed explanations are very case-specific [11,12]. Moreover, evidence suggests that surface phenomena are not only able to hinder the transport inside the pore but on the opposite facilitate it, especially for the molecules that strongly interact with a zeolite framework [13]. In addition, in a large-scale industrial catalysis, gas transport is also influenced by zeolite-shaping additives, operating conditions, and time-on-stream [1].

Advanced model materials [14] and multi-scale computational models [15,16] can in principle capture some of the aforementioned complexities of transport in zeolites, but more robust and

* Corresponding author.
E-mail address: evgeniyr@smn.uio.no (E. Redekop).

https://doi.org/10.1016/j.cattod.2022.05.050
Received 7 February 2022; Received in revised form 9 May 2022; Accepted 31 May 2022
Available online 9 June 2022

Nomenclature

A	cross-sectional area of the TAP reactor bed, m^2;.
A_S	concentration of surface active sites, mol/m^2.
C	gas concentration, mol/m^3;.
$\overline{C}$	dimensionless concentration of gas;.
C_p	gas concentration inside micropores, mol/m^3;.
$\overline{C_p}$	dimensionless gas concentration inside micropores;.
D_b	bulk diffusivity through TAP reactor bed, m^2/s;.
D_p	intracrystalline diffusivity within zeolite crystal, m^2/s;.
k_a	adsorption rate on the surface active sites, $m^3/(mol \cdot s)$;.
$\overline{k_a}$	dimensionless adsorption rate on the surface active sites;.
k_d	desorption rate from the surface active sites, s^{-1};.
$\overline{k_d}$	dimensionless desorption rate from the surface active sites;.
$k_{a(int)}$	adsorption rate inside confined space of micropores, $m^3/(mol \cdot s)$;.
$\overline{k_{a(int)}}$	dimensionless adsorption rate inside confined space of micropores;.
$k_{d(int)}$	desorption rate inside confined space of micropores, s^{-1};.
$\overline{k_{d(int)}}$	dimensionless desorption rate inside confined space of micropores;.
k_{ent}	gas pore entrance (intake) rate, s^{-1};.
$\overline{k_{ent}}$	dimensionless gas pore entrance (intake) rate;.
k_{ext}	gas pore exit (outtake) rate, s^{-1};.
$\overline{k_{ext}}$	dimensionless gas pore exit (outtake) rate;.
K_H	equilibrium adsorption constant, Henry constant;.
L	length of TAP reactor, m;.
N	amount of gas pulsed through the reactor, mol;.
r	spatial coordinate of zeolite crystal, m;.
S_v	surface to volume ratio of zeolite crystal, m^{-1};.
t	time, s;.
z	spatial coordinate of TAP reactor bed, m.

Greek letters

α	ratio of the characteristic interpellet bed diffusion time and the characteristic intrapellet pellet diffusion time, dimensionless;.
β	geometric factor of zeolite crystal, dimensionless;.
δ	ratio of the zeoltie crystal radius to the thickness of the single-unit layer on the outer tim of the crystal; dimensionless;.
δ_Z	Dirac delta function of reactor length space;.
Δl	unit-cell thickness of surface layer of zeolite;.
ε_b	bulk porosity of the TAP reactor bed, dimensionless;.
ε_p	porosity within the zeolite (catalyst) crystal (ratio of void volume to total crystal volume, dimensionless;.
θ	surface coverage, dimensionless;.
$\overline{\theta}$	dimensionless surface coverage;.
ζ	dimensionless spatial coordinate of TAP reactor;.
ρ	dimensionless radial coordinate of zeolite crystal;.
τ	dimensionless time.

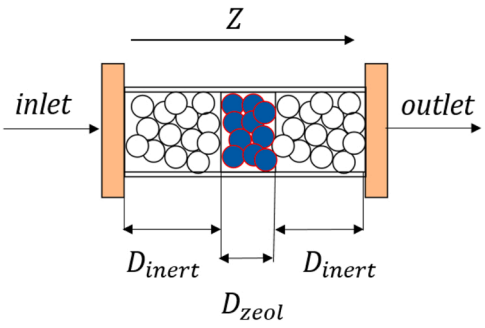

Fig. 1. Schematics of three Zone TAP reactor.

computationally tractable models are more suitable for the routine regression of transient kinetic data for catalytic reactions. These models of "optimal complexity" [17] must adequately and accurately represent the essential features of transient responses at appropriate time scales without either under- or over-fitting the data. Only then can the intrinsic parameters of diffusion, adsorption, and reactions be properly estimated by data regression.

The Transient Analysis of Products (TAP) technique is uniquely suited for gathering transient intrinsic kinetics data in zeolites, among a wide range of materials [4,5]. Classical TAP experiments are conducted under low-pressure conditions, whether the reactor-scale gas transport occurs by well-defined Knudsen diffusion, and a temporal resolution of milliseconds. Furthermore, TAP measurements can be combined, within the same device and for the same sample, with steady-state and non-steady-state experiments under various other conditions. This approach can accommodate materials of vastly different complexities, including pristine well-defined zeolites, hierarchical materials, and application-ready porous pellets. The scope of TAP applications in zeolite catalysis includes gas adsorption and diffusion [18–20], dehydration reactions [21], hydrocarbon conversion [22], cracking and reforming [23], MTH and MTO processes [1,24–26].

In this paper, we extend the range of transport models used for the analysis of TAP data with microporous diffusion [2,27,28] by incorporating terms that reflect surface barriers and complex nature of microporous diffusion. Numerical studies were used to map sensitivity ranges of increasingly detailed models, and novel fingerprints were identified in model behavior that can aid in data interpretation for future experiments.

2. Methodology

2.1. Standard TAP model

Configuration of TAP reactor that is typically used for investigation of reactions catalyzed by microporous materials is illustrated in Fig. 1. Reactor consists of 3 zones: two inert zones that are usually filled with inert material like quartz and one catalytic zone in the middle filled with, for example, zeolite. The length of catalytic zone can be adjusted to control the amount of catalyst, hence the contact time with pulsed gas. Diffusion length of the passing molecules can also be controlled by adjusting the length of zones and selecting materials of certain bulk porosity. Suitable reactor design justifies the assumption of negligible radial concentration gradients, radial and axial temperature gradients and, most importantly, that gas diffusivity within each zone is constant, which is ensured by using a relatively narrow fraction of particle sizes (usually sieved to $250 < d < 400\mu m$). In practice, experiments are typically conducted in thin-zone configuration of the reactor to minimize non-uniformities of concentration and ensure that the catalyst zone is positioned in the isothermal reactor zone. More details about testing and validating these assumptions are presented elsewhere [29–32,33]. For gases that do not experience microporous diffusion delay and do not interact with catalyst, the model is a simple one-dimensional diffusion equation in heterogeneous media. Initial conditions for the partial differential equation assume the gas pulse in the inlet of the reactor at time

zero can be described as Dirac delta function. Neumann and Dirichlet boundary conditions imply zero influx at the inlet of the reactor and zero gas concentration at the outlet. The reactor assembly and simple model provide robust basis for estimation of Knudsen diffusivity of gases.

$$\varepsilon_b \frac{\partial C_A}{\partial t} = D_{bA} \frac{\partial^2 C_A}{\partial z^2} \tag{1}$$

With initial conditions:

$$0 \le z \le L, \qquad t = 0, \qquad C_A = \delta_Z \frac{N_A}{\epsilon_b A}; \tag{2}$$

And boundary conditions:

$$\begin{aligned} z &= 0, \quad \frac{\partial C_A}{\partial z} = 0; \\ z &= L, \quad C_A = 0; \end{aligned} \tag{3}$$

2.2. Development of mathematical models

2.2.1. Model 1. Equilibrium adsorption at the pore mouth + microporous diffusion (EqMP)

The 2-parameter model of microporous diffusion in the TAP context, originally proposed by Keipert [27], was selected as a benchmark model. The gas transport inside the pore is controlled by a Henry-like constant of adsorption equilibrium at the pore mouth K_H and microporous diffusivity D_p. Distribution of gas molecules along the micropores is described in this model by the transient one-dimensional 2nd Fick's law. Pores are assumed equal-sized and evenly distributed forming a pseudo-homogeneous environment within the crystallite. Potentially differing modes of diffusion are described by a single microporous diffusivity D_p which is assumed isotropic and homogeneous through the zeolite crystal. Intracrystalline diffusion within the zeolite particle is assumed symmetrical in relation to the crystal centre and for crystals with 1D pore architecture the diffusion equation can be implemented in linear coordinates, while for 3D pore systems spherical coordinate system can be applied. Gas transport between crystals is assumed to always follow bulk Knudsen diffusivity. The underlying assumption in all models developed herein is that equally-sized pores are distributed isotropically and homogeneously within the crystallite, forming a pseudo-homogeneous diffusion domain. This assumption makes the models valid at least for two broad classes of microporous materials often encountered in practice: 1D parallel pores (e.g. TON, AFI) and 3D highly-interconnected pores of equal diameter (e.g. MFI) or cavities interconnected by windows (e.g. CHA, AEI). Other types of materials in which interconnected pore systems with multiple sizes exist may require more intricate models to be developed.

$$\varepsilon_b \frac{\partial C_A}{\partial t} = D_{bA} \frac{\partial^2 C_A}{\partial z^2} - (1-\varepsilon_b) S_v D_p \frac{\partial C_{pA}}{\partial r}\Big|_{r=R} \tag{4}$$

Intra-pellet diffusion inside rectangular pellets is defined as:

$$\varepsilon_p \frac{\partial C_p}{\partial t} = D_p \frac{\partial^2 C_p}{\partial r^2} \tag{5}$$

With initial conditions:

$$t = 0, \qquad C_A = \delta_Z \frac{N_A}{\epsilon_b A}, \qquad C_{pA} = 0. \tag{6}$$

And boundary conditions:

$$\begin{aligned} z &= 0, \quad \frac{\partial C_A}{\partial z} = 0; \\ z &= L, \quad C_A = 0; \\ r &= 0, \quad \frac{\partial C_{pA}}{\partial r} = 0; \\ r &= R, \quad C_{pA} = K_H C_A. \end{aligned} \tag{7}$$

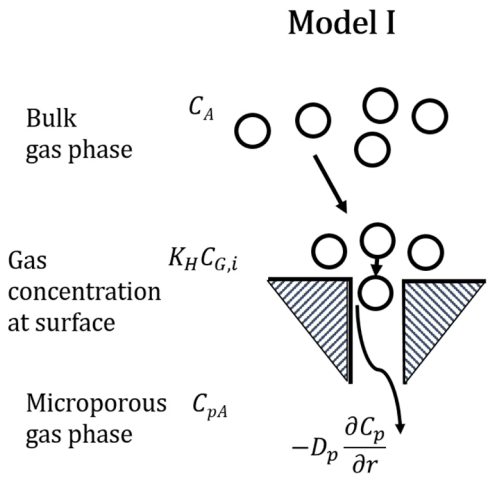

Fig. 2. Concept of Equilibrium adsorption + microporous diffusion model.

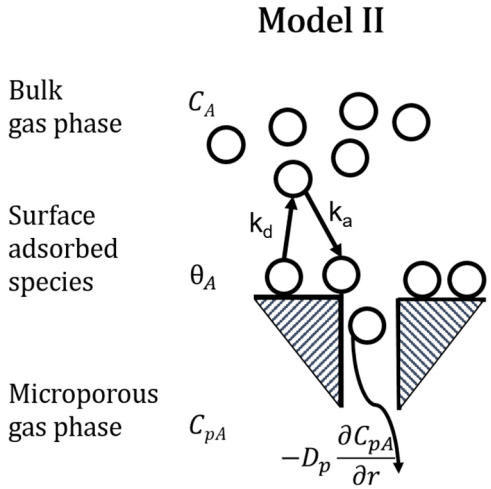

Fig. 3. Concept of dynamic adsorption + microporous diffusion model.

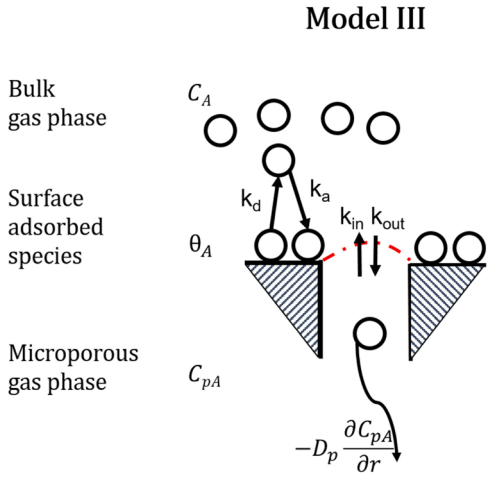

Fig. 4. Concept of dynamic adsorption + surface barriers model.

This model is simple, robust and captures well experimental data on the transport of light inert, permanent, and hydrocarbon gases through several zeolites, although primarily these examples involve relatively weakly interacting pairs of gases and materials (e.g. alkanes and alkene

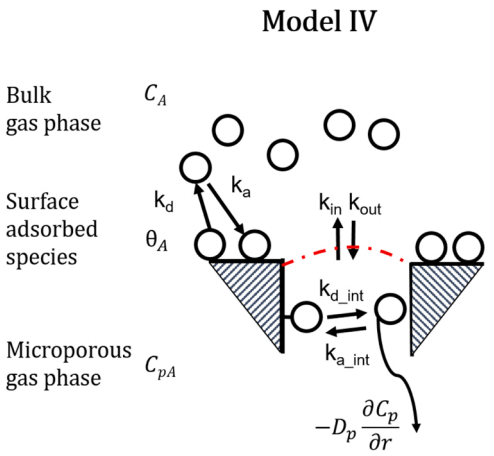

Fig. 5. Concept of dynamic adsorption + surface barriers model and microporous adsorption model.

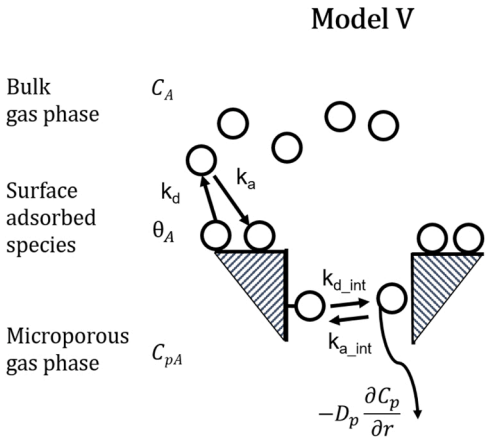

Fig. 6. Concept of dynamic surface adsorption + microporous adsorption model.

in neutral silicalites and alkanes in acidic zeolites). The model features only two parameters (in addition to bulk diffusivities in the packing zones) that need to be regressed - K_H and D_p. Therefore, it is fairly easy to perform explicit sensitivity analysis of this model and use it as a benchmarking example for other models Figs. 2, 3, 4, 5, 6.

2.2.2. Model 2. Dynamic adsorption, microporous diffusion model (DAMP)

Further extension of the Keipert's model considers dynamic, i.e. non-equilibrated, adsorption at the pore mouth prior to pore diffusion, as reflected by two parameters - adsorption constant k_a and desorption constant k_d [2,6]. Non-equilibrated adsorption explicitly accounts for the existence of a finite capacitance corresponding to the coverage of the adsorbate at the outer surface of a zeolite, which is reflected by a dedicated spatially-localized variable θ_A. This adsorbate capacitance at the outer surface can simultaneously and dynamically (i.e. non-equilibrated at the time scales of the experiment involved) exchange with the bulk as well as microporous domains. Importantly, the model with a finite dynamic capacitance allows accurate representation of cases in which strong adsorption at the outer surface may result in a measurable delay of the probe molecule with respect to the inert standard, even without the pore entry. It can also account for the limitation of diffusion into the pores by the insufficient amount of adsorption sites at the outer surface. In comparison, Model 1 assumes instant equilibrium between the probe molecules in the bulk and the boundary layer of the pseudo-homogeneous pore space, thus failing to account for the subtle transient effects related to changes of the coverage at the outer surface.

We note that the concept of a unit cell thickness defined in boundary conditions may not apply in many cases of practical importance, e.g. disordered microporous materials such as activated carbon, which are not considered in this work.

$$\begin{aligned} \varepsilon_b \frac{\partial C_A}{\partial t} &= D_{bA} \frac{\partial^2 C_A}{\partial z^2} - A_S S_v (1-\varepsilon_b)(k_a C_A (1-\theta_A) - k_d \theta_A) \\ \frac{\partial \theta_A}{\partial t} &= k_a C_A (1-\theta_A) - k_d \theta_A - \frac{D_p}{A_S} \frac{\partial C_p}{\partial r}\Big|_{r=R} \end{aligned} \tag{8}$$

$$\varepsilon_p \frac{\partial C_p}{\partial t} = D_p \frac{\partial^2 C_p}{\partial r^2} \tag{9}$$

With initial conditions:

$$t = 0, \qquad C_A = \delta_Z \frac{N_A}{\epsilon_b A}, \qquad \theta_A = 0, \qquad C_{pA} = 0. \tag{10}$$

And boundary conditions:

$$\begin{aligned} z &= 0, & \frac{\partial C_A}{\partial z} &= 0; \\ z &= L, & C_A &= 0; \\ r &= 0, & \frac{\partial C_{pA}}{\partial r} &= 0; \\ r &= R, & \varepsilon_p C_{pA} &= \frac{A_S}{\Delta l} \theta_A. \end{aligned} \tag{11}$$

The model describes the distribution of gas molecules within micropores in a similar fashion to Keipert model.

2.2.3. Models 3 - Dynamic adsorption, surface barriers model (DASB). Model 4 - Dynamic adsorption, surface barriers + dynamic microporous adsorption (DASBMA) model

Models reflecting the surface barriers were developed on the basis of the dynamic adsorption model. Concentration of adsorbed molecules on the outer surface of zeolite crystal is represented by the surface coverage as in case of the previous model, however, to reflect surface barriers or facilitated transport, the intake and outtake rate through the pore mouth were introduced. The rates are defined by two constants k_{ent} and k_{ext} accordingly. Microporous transport is described by the single diffusivity term D_p as in the previous models.

The transport equation for model reflecting surface barriers:

$$\begin{aligned} \varepsilon_b \frac{\partial C_A}{\partial t} &= D_{bA} \frac{\partial^2 C_A}{\partial z^2} - A_S S_v (1-\varepsilon_b)(k_a C_A (1-\theta_A) - k_d \theta_A) \\ \frac{\partial \theta_A}{\partial t} &= (k_a C_A (1-\theta_A) - k_d \theta_A) - k_{ent} \theta_A + \frac{\varepsilon_p}{A_S S_v} k_{ext} C_{pA}|_{r=R} \end{aligned} \tag{12}$$

$$\varepsilon_p \frac{\partial C_{pA}}{\partial t} = D_{pA} \frac{\partial^2 C_{pA}}{\partial r^2} \tag{13}$$

With initial conditions:

$$t = 0, \qquad C_A = \delta_D \frac{N_A}{\epsilon_b A}, \qquad \theta_A = 0, \qquad C_{pA} = 0. \tag{14}$$

And boundary conditions:

$$\begin{aligned} z &= 0, & \frac{\partial C_A}{\partial z} &= 0; \\ z &= L, & C_A &= 0; \\ r &= 0, & \frac{\partial C_{pA}}{\partial r} &= 0; \\ r &= R, & D_p \frac{\partial C_{pA}}{\partial r} &= k_{ent} A_S \theta_A - \frac{1}{S_v} k_{ext} \varepsilon_p C_{pA}|_{r=R}. \end{aligned} \tag{15}$$

In certain systems, mixing several modes of diffusion into a single parameter may result in misleading estimated values of diffusivity. For example, the estimated activation energy of Knudsen diffusion is within

the range 6–10▓kJ/mol [3], meanwhile, surface diffusivity - an alternative transport mode on the outer surfaces or mesopores, can reach up to 20–40▓kJ/mol [34]; single-file diffusion in narrow channels does not exhibit Arrhenius type dependency per se [35]. In cases where different transport regimes coexist, the diffusivity coefficient can deviate from standard Arrhenius dependency, thus disentangling different diffusivities from a single term can provide more accurate and consistent data. Following the idea, the microporous diffusivity, that was represented by single term in previous models, in Model 4 is represented by 3 terms that reflect both random-motion character of diffusion (D_p) and surface hopping character ($k_{a(int)}$ and $k_{d(int)}$) (Eq. 17).

$$\begin{aligned}\varepsilon_b\frac{\partial C_A}{\partial t} &= D_{bA}\frac{\partial^2 C_A}{\partial z^2} - A_S S_v(1-\varepsilon_b)(k_a C_A(1-\theta_A) - k_d\theta_A)\\ \frac{\partial \theta_A}{\partial t} &= (k_a C_A(1-\theta_A) - k_d\theta_A) - k_{ent}\theta_A + \frac{\varepsilon_p}{A_S S_v}k_{ext}C_{pA}|_{r=R}\end{aligned} \tag{16}$$

$$\begin{aligned}\varepsilon_p\frac{\partial C_{pA}}{\partial t} &= D_{pA}\frac{\partial^2 C_{pA}}{\partial r^2} - A_{S(int)}(k_{a(int)}C_{pA}(1-\theta_{A(int)}) - k_{d(int)}\theta_{A(int)})\\ \frac{\partial \theta_{A(int)}}{\partial t} &= (k_{a(int)}C_{pA}(1-\theta_{A(int)}) - k_{d(int)}\theta_{A(int)})\end{aligned} \tag{17}$$

With initial conditions:

$$t=0,\qquad C_A = \delta_Z\frac{N_A}{\epsilon_b A},\qquad \theta_A = 0,\qquad C_{pA}=0,\qquad \theta_{A(int)}=0. \tag{18}$$

The boundary conditions repeat boundary conditions of surface barrier model in Eq. (15).

2.2.4. Model 5. Dynamic surface adsorption and microporous adsorption (DSAMA)

This model was developed as a simplified version of Model 4, that still captures the complex nature of microporous diffusion but ignores the presence of transport hindrances at pore mouth. The model was designed to describe transport in systems with strong internal adsorption and large $R_{pore}/R_{molecule}$ ratio. No resistance at pore mouth implies that terms k_{ent} and k_{ext} can be omitted. Microporous transport in this model follows two steps: 1) pre-adosprtion on the surface of zeolites and 2) transport within the pore by activated surface and random motion diffusion:

$$\begin{aligned}\varepsilon_b\frac{\partial C_A}{\partial t} &= D_{bA}\frac{\partial^2 C_A}{\partial z^2} - A_S S_v(1-\varepsilon_b)(k_a C_A(1-\theta_A) - k_d\theta_A)\\ \frac{\partial \theta_A}{\partial t} &= k_a C_A(1-\theta_A) - k_d\theta_A - \frac{D_p}{A_S}\frac{\partial C_p}{\partial r}|_{r=R}\end{aligned} \tag{19}$$

$$\begin{aligned}\varepsilon_p\frac{\partial C_{pA}}{\partial t} &= D_{pA}\frac{\partial^2 C_{pA}}{\partial r^2} - A_{S(int)}(k_{a(int)}C_{pA}(1-\theta_{A(int)}) - k_{d(int)}\theta_{A(int)})\\ \frac{\partial \theta_{A(int)}}{\partial t} &= (k_{a(int)}C_{pA}(1-\theta_{A(int)}) - k_{d(int)}\theta_{A(int)})\end{aligned} \tag{20}$$

With initial conditions:

$$t=0,\qquad C_A = \delta_D\frac{N_A}{\epsilon_b A},\qquad \theta_A = 0,\qquad C_{pA}=0,\qquad \theta_{A(int)}=0. \tag{21}$$

The boundary conditions repeats boundary conditions of Model 2 in Eq. (11).

2.3. Dimensionless models

Even though that current computational capacity allows numerical solution of presented models on a generally available office PC, to conduct a sensitivity study of 3-, 5-, 7-parametric models requires hundred of thousands simulations which consume great amount of time. Analytical solutions are far more attractive options in these terms, however, due to heterogeneous non-linear character of models, it is a voluminous task to provide analytical solution, unless some simplifications are made. To remove heterogeneity, the reactor is assumed to contain only 1 Zone - catalytic. In order to linearize models, assumption of $\theta_A << 1$ was introduced, thus, the term $(1-\theta_A)$ could be removed from mathematical expression. Following the approach presented by Colaris [28], we developed dimensionless models for 1 Zone reactor and found solutions using inverse Laplace transformation. The resulting analytical expressions can be used more efficiently for the sensitivity studies, while reflecting the same trends as those observed in more realistic three-zone models. In this section, we present the final solutions to the Laplace-transformed dimensionless models.

Keipert model (Model 1) defines dimensionless flow as:

$$\begin{aligned}\overline{Flow} &= cosh(\sqrt{f(s)+s}\,)\\ f(s) &= \alpha\beta K_H\frac{(1-\varepsilon_b)\varepsilon_p}{\varepsilon_b}\gamma(s)tanh(\gamma(s))\\ \gamma(s) &= \sqrt{\frac{s}{\alpha}}\end{aligned} \tag{22}$$

Model 2. Dynamic adsorption microporous diffusion model (DAMP):

$$\begin{aligned}\overline{Flow} &= cosh(\sqrt{f(s)+s}\,)\\ f(s) &= \frac{\overline{k_a}(s+\varphi(s))}{s+\overline{k_d}+\varphi(s)}\\ \varphi(s) &= \alpha\delta\gamma(s)tanh(\gamma(s))\\ \gamma(s) &= \sqrt{\frac{s}{\alpha}}\end{aligned} \tag{23}$$

Model 3. Surface barriers and micropore diffusion model (DASB):

$$\begin{aligned}\overline{Flow} &= cosh(\sqrt{f(s)+s}\,)\\ f(s) &= \frac{\overline{k_a}(s+\varphi(s))}{s+\overline{k_d}+\varphi(s)}\\ \varphi(s) &= \frac{\overline{k_{ent}}}{1+\frac{\overline{k_{ent}}}{\alpha\beta\gamma(s)tanh(\gamma(s))}}\\ \gamma(s) &= \sqrt{\frac{s}{\alpha}}\end{aligned} \tag{24}$$

Model 4. Surface barriers and decoupled micropore diffusion with internal adsorption model (DASBMA):

$$\begin{aligned}\overline{Flow} &= cosh(\sqrt{f(s)+s}\,)\\ f(s) &= \frac{\overline{k_a}(s+\varphi(s))}{s+\overline{k_d}+\varphi(s)}\\ \varphi(s) &= \frac{\overline{k_{ent}}}{1+\frac{\overline{k_{ent}}}{\alpha\beta\gamma(s)tanh(\gamma(s))}}\\ \gamma(s) &= \sqrt{\frac{s}{\alpha}\left(1+\frac{\overline{k_{a(int)}}}{\frac{s}{\alpha}+\overline{k_{d(int)}}}\right)}\end{aligned} \tag{25}$$

Model 5. Dynamic surface and internal adsorption model (DSAMA):

$$\begin{aligned}\overline{Flow} &= cosh(\sqrt{f(s)+s}\,)\\ f(s) &= \frac{\overline{k_a}(s+\varphi(s))}{s+\overline{k_d}+\varphi(s)}\\ \varphi(s) &= \alpha\delta\gamma(s)tanh(\gamma(s))\\ \gamma(s) &= \sqrt{\frac{s}{\alpha}\left(1+\frac{\overline{k_{a(int)}}}{\frac{s}{\alpha}+\overline{k_{d(int)}}}\right)}\end{aligned} \tag{26}$$

Studying dimensionless models is beneficial in many ways. First of all, dimensionless models have a reduced number of parameters. For example, we do not have to consider the influence of bulk diffusivity, bed porosity and length scale of the reactor itself since in dimensionless models those parameters are accounted for in dimensionless time variable and incorporated in corresponding dimensionless parameters. Secondly, the variables that dimensionless models can provide insights on the importance of ratios between parameters that otherwise remain hidden. For example, the dimensionless variable that reflects ratio between characteristic time of bulk diffusion and time of microporous diffusion α or variable β, that reflects the geometric factor of crystal shape. On the other hand, using a 1 Zone model provides a higher sensitivity to the change of parameters, which in the case of 3 Zone model would be smoothed out by the introduction of 2 inert zones. Overall, extrapolating the data on the 3 Zone model should be done with caution and more narrow sensitivity ranges are to be expected in comparison with a 1 Zone model.

Last, but not least, dimensionless models are scale-invariant, making the results of their analysis applicable across a wide range of spatio-temporal dimensions. For example, conclusions on model sensitivity derived from our results can be straightforwardly adopted to TAP microreactors of different lengths/diameters from different laboratories. Likewise, the dimensionless analysis can, in principle, be applied to better understand adsorption and diffusion in materials with extra scales of porosity, e.g. hierarchical zeolites [3], although herein we consider only two length scales of diffusion: a pseudo-homogeneous reactor-scale domain of macroporous and interstitial diffusion and another pseudo-homogeneous pore-scale domain of microporous diffusion inside zeolitic crystallites.

2.4. Thermodynamic influence analysis

The influence of adsorption thermodynamics on the behavior of the proposed models was elucidated by analyzing the dependency of the mean residence time (MRT) on the change in temperature. Mean residence time is defined as ratio between first and zeroth moment (Eq. 27). Tracking MRT as a function of temperature, alongside with the zeroth moment, is commonly employed in TAP experiments to investigate adsorption and reaction thermodynamics [19,24,27]. MRT offers a convenient descriptor because it has a clear physical meaning, easy to extract from pulse-response data, and reflects well the kinetic and thermodynamic dependencies.

$$MRT = \frac{\int_0^\infty F_A t dt}{\int_0^\infty F_A dt} \tag{27}$$

Since the temperature dependency of surface permeation coefficients is still unclear, due to diverse origin of surface barriers, the study was performed on models that do not contain permeation rates (k_{ent} and k_{ext}) - Model 2 (DAMP) and Model 5 (DSAMA). The desorption rate coefficients for both, external and internal active sites were estimated from the assumed equilibrium constant using thermodynamic consistency (28, 29), with the adsorption rate coefficients prescribed according to the Hertz-Knudsen equation (30, 31). The sticking coefficient set to $\chi = 0.3$ [36]. Bulk diffusivity followed Knudsen square root temperature dependency (32), meanwhile microporous diffusivity exponentially depended on temperature (33) which is typical for activated surface diffusion.

$$K_{eq} = exp\left(-\frac{\Delta H_{ads} - T\Delta S_{ads}}{RT}\right) \tag{28}$$

$$K_{eq} = \frac{k_{ads}}{k_{des}} \tag{29}$$

$$\frac{1}{A}\frac{dN}{dt} = \frac{\chi p N_A}{\sqrt{2\pi MRT}} \tag{30}$$

$$k_a = \frac{\chi \varepsilon_b}{A_S(1-\varepsilon_b)}\sqrt{\frac{RT}{2\pi M}} \tag{31}$$

$$D_b = \frac{\lambda}{3}\sqrt{\frac{8RT}{\pi M}} \tag{32}$$

$$D_p = D_{p0}\exp\left(-\frac{E_{diff}}{RT}\right) \tag{33}$$

Typical ranges of the activation energy for microporous diffusion as well as the enthalpy and entropy of adsorption were obtained from the literature. Based on ab initio modeling of iso-butane adsorption on ZSM-5 zeolite [37,38], appropriate starting set of thermodynamic parameters was selected as: $\Delta H_{ads} = -40 kJ/mol$, $\Delta S_{ads} = -100 J/mol/K$. For clearer representation of trends, a higher value of $\Delta S_{ads} = -150 J/mol/K$ was used to simulate the temperature dependency of MRT at different E_{diff}. Thermodynamic parameters of adsorption on internal active sites were defined as $\Delta H_{ads(int)} = \Delta H_{ads} + \Delta\Delta H_{ads}$ and $\Delta S_{ads(int)} = \Delta S_{ads} + \Delta\Delta S_{ads}$. For cases where these parameters were not varied, they were assigned constant values with $\Delta\Delta H_{ads} = 0 kJ/mol$ and $\Delta\Delta S_{ads} = -20 J/mol/K$. The initial values for the activation energy of microporous diffusion were also adopted from measurements of isobutane adsorption on ZSM-5, as reflected in Keipert work [27]: $E_{diff} = 25 kJ/mol$, $D_{p0} = 10^{-11} m^2/s$.

2.5. Sensitivity metrics

The choice of sensitivity metric is essential when exploring mathematical models in the parameter space. Here, two approaches were used for this purpose: curve shape descriptors commonly used in the TAP literature and global first derivative search [39–42]. Previous sensitivity studies of microporous diffusion models in the context of TAP experiments represented the pulse-response shapes by 3 properties: MRT, pulse peak time, and pulse dispersion. Visual inspection of gradients in these descriptors in multi-dimensional parametric space was then used as nominal sensitivity metrics. To this end, a modified global derivatives search was used for the parametric sensitivity study [40,41]. In the latter case, we defined sensitivity to a certain parameter as the first derivative of the flow along *Log10* of the parameter. The log space was used to accommodate the vast range of parameter magnitudes explored, even for dimensionless kinetic and diffusion variables.

$$Sens = \frac{d\overline{F}}{dlog(par)} = \frac{1}{N-1}\frac{\sum_0^N \left|\overline{F}_{par()n+1} - \overline{F}_{par(n)}\right|}{log(h)} \tag{34}$$

For 2D plots presented in the results section, the derivative was calculated as an average between two derivatives along different axes:

$$Sens_{2D} = \frac{1}{2}\left(\frac{d\overline{F}}{dlog(par_1)} + \frac{d\overline{F}}{dlog(par_2)}\right) \tag{35}$$

Global first derivative search is a commonly utilized method in studying model sensitivity in chemical and bio-engineering [37]. Especially, it was proven as a useful tool in the field of convoluted and heterogeneous models where parameters cannot be delineated from each other.

2.6. Regression procedure

Non-linear regression of the pulse-response transients was performed using the *scipy* Python package. Since regression is conducted in the environment of physically bonded parameters in a narrow range of *Log10* parameter variation, the Dogbox method was chosen. The soft L1 (absolute difference) norm was chosen as a loss function to emphasize the data in the tail of the flow curve. Since the tail of pulse-response signal approaches zero, the residual function, which is defined as a difference between simulated and regressed response, in the tail

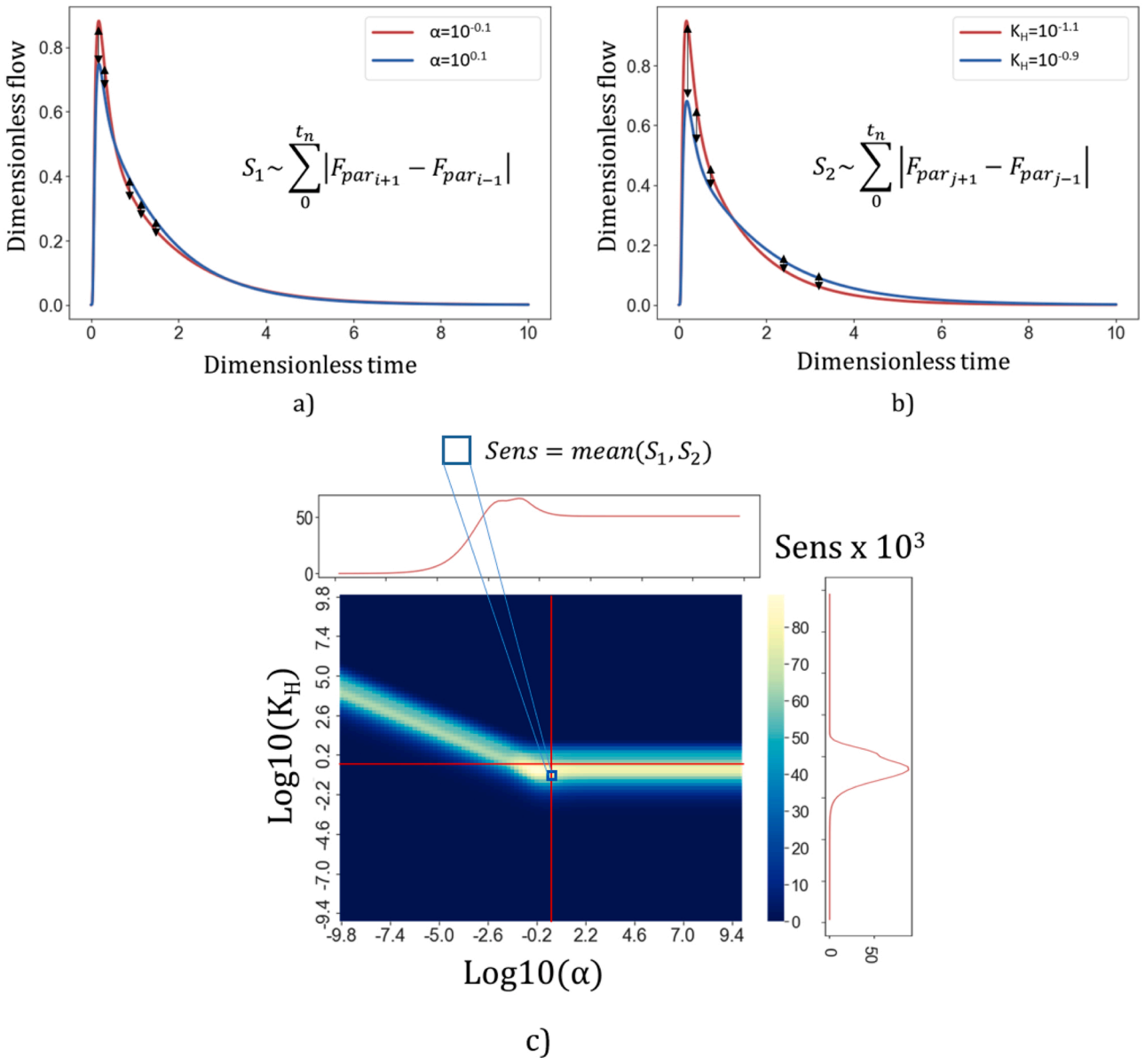

Fig. 7. Sensitivity plot of Keipert 2-parametric model and step-by-step schematics on how it was obtained. a) Pulse-response curves obtained by variation of α parameter, S_1 - the integral flow change due to the change of α variable; b) Pulse-response curves obtained by variation of K_H parameter, S_2 - the integral flow change due to the change of K_H variable; c) Sensitivity plot, single pixel reflects averaged integral flow change due to the change of variables.

approaches zero at even faster rates. Thus, L2 norm would square already a small difference ($< < 1$). This will result in the regression engine searching for set of parameters that primarily minimize residual in the region of large difference such as peak area, ignoring minor difference in the tails. Meanwhile, it is the tail of the pulse-response curve that reflects the microporous diffusion delay.

3. Results and discussion

3.1. Sensitivity study

In this section, enhanced models that reflect complex hydrocarbon transport in greater detail are examined for their parametric sensitivity. This study aimed to provide insights on how additional parameters influence the sensitivity ranges to other parameters and demarcate the regions of parametric space where developed models are feasible for capturing pulse-response curves.

Keipert model provides a convenient starting point and a benchmark before sensitivity ranges of more complex models can be explored. There are only two parameters in the Keipert model - K_H and D_p, thus sensitivity can be visualized on a 2D surface plot. In dimensionless coordinates, D_p is represented as the α coefficient.

In the 2D sensitivity plot (Fig. 7) of the Keipert model, three characteristic regions can be observed: i) the narrow central region (high-intensity band) where model is sensitive to the parameter values; ii) the region above the sensitivity band where irreversible adsorption precludes the probe molecules from exiting the reactor; iii) the region below the sensitivity band where adsorption is too weak to induce a measurable delay in the pulse-response data in comparison to the inert Standard Diffusion Curve (SDC). Sensitivity band itself can be subdivided into two arms with a clear change of slope in between that occurs at ca. $log(\alpha) = 0$. The left arm with $log(\alpha) < 0$ signifies the model sensitivity to both α and K_H parameters, while the right arm with $log(\alpha) > 0$ is sensitive only to K_H. The value of $log(\alpha) > 0$ implies that the characteristic timescale of bulk diffusion is greater than that of microporous diffusion and that the concentration gradient along the pore is established faster than the

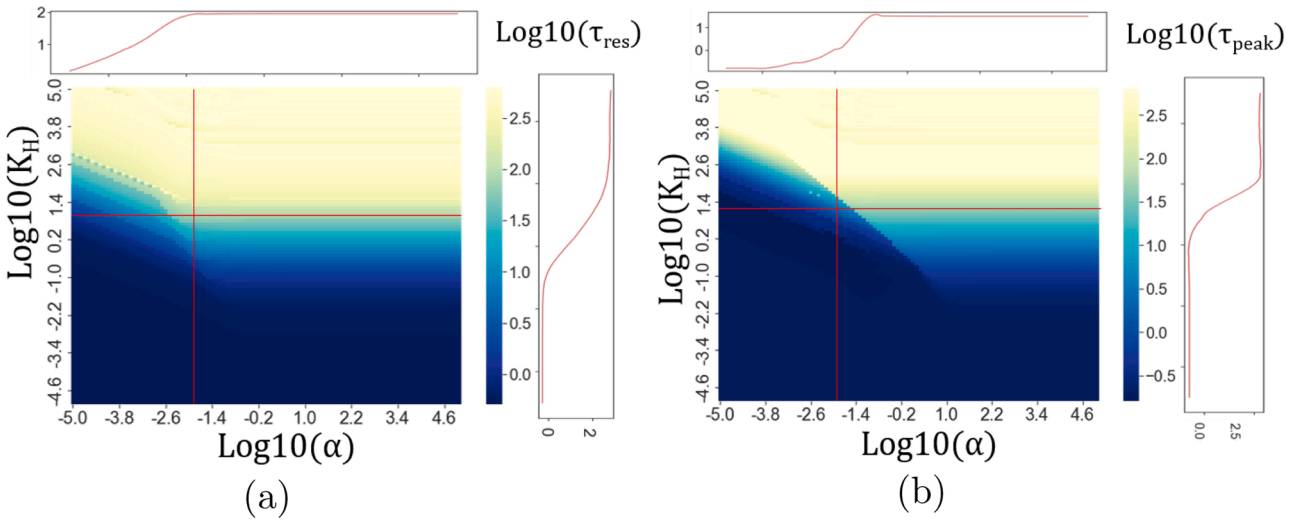

Fig. 8. Mean residence time (MRT) and peak time (PT) parametric sensitivity of Keipert model.

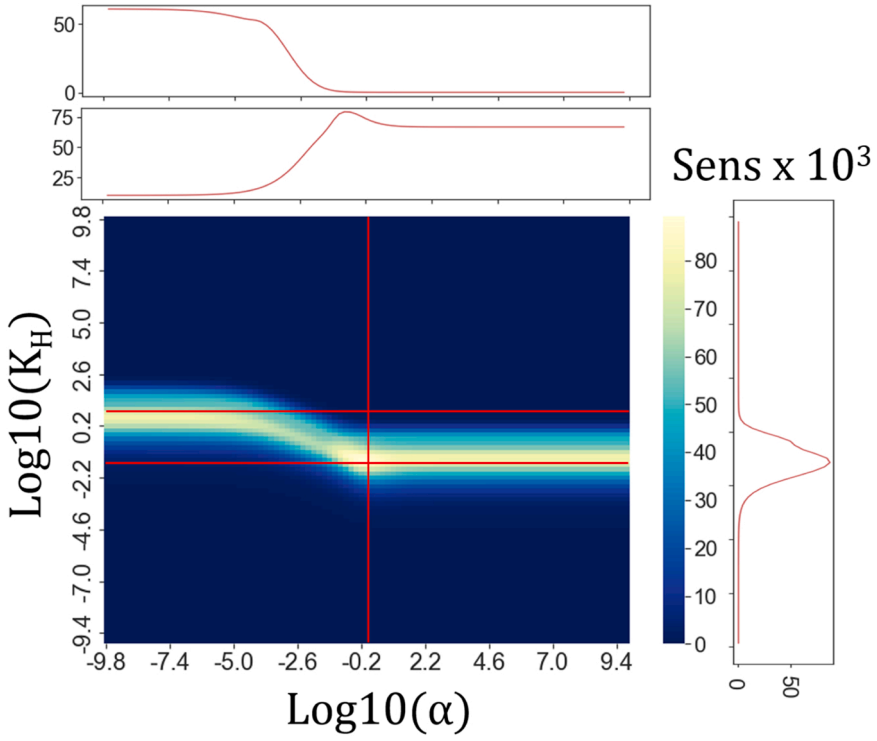

Fig. 9. Sensitivity plots of dynamic adsorption microporous diffusion models at $\overline{k_a} = 10^4$.

concentration gradient along the reactor bed. This analysis is fully consistent with Keipert et al. [27] and clearly illustrates that bulk diffusion in TAP experiments cannot be used as a sensitive measure of microporous transport, unless the combination of geometric and transport parameters place it inside the prescribed sensitivity band. We note that attempts to visually correlate our sensitivity metric to the first derivatives of *log*(*MRT*) and *log*(*PT*) used in the original analysis by Keipert et al [27]. did not reveal a straightforward correlation between the two frameworks of sensitivity descriptors, aside from the general bounds on the sensitivity regions Fig. 8.

In order to illustrate how the data on Fig. 7 can assist experimental design, we conducted a simulation study (see Supplementary Information section 3) in which isobutane was pulsed through H-ZSM5 zeolite in 1 Zone TAP reactor. Typical settings of experimental setup demonstrated that operating window is out of microporous diffusivity sensitivity range. To shit the operating window, adjustment strategies can be applied: shorten the length of the catalytic zone and increase the size fraction of the catalyst particles to effectively adjust bulk diffusion length. Or, alternatively, select material with larger size of crystallites to increase intracrystalline diffusion length. Common goal of these strategies is to increase time-scale of microporous diffusion and reduce time-scale of bulk diffusion.

The model extended with dynamic (i.e. not necessarily non-equilibrated) adsorption at the pore mouth exhibits a different behavior of the sensitivity metric (Fig. 9). Here, results are presented in a familiar two-dimensional view for a fixed value of the adsorption rate coefficient, while the two other parameters $\overline{k_d}$ and α are varied. Although generally similar to the Keipert model, the sensitivity band

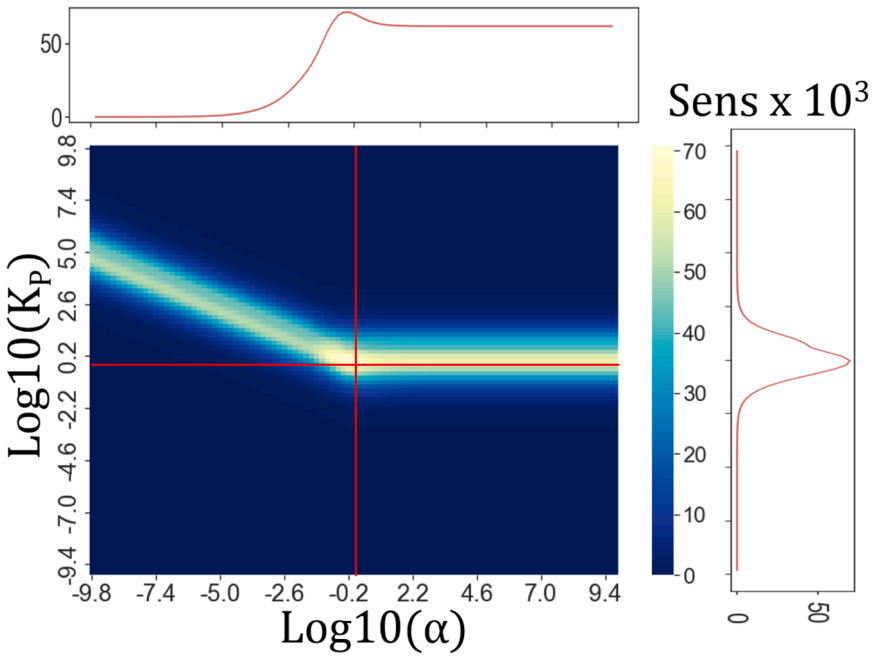

Fig. 10. Sensitivity plots of surface barriers microporous diffusion model reflecting the change of $\overline{k_{ent}}/\overline{k_{ext}}(K_P)$ ratio at different α.

structure for this model is distinctly different in shape, especially in the left arm with $\alpha < 10^{-5}$. The origin of this difference in the sensitivity band structure with respect to the Keipert model can be traced to the presence of an additional (monolayer) adsorption capacity at the outer pore mouth required in the dynamic model. For very slow microporous diffusion, the interplay of the finite adsorption/desorption rates into and out of this additional capacity accounts for the variation of pulse-response and precludes the model sensitivity towards microporous diffusion.

The influence of the $\overline{k_a}$ values on the extent and shape of the sensitivity band was evaluated within $10^{-2}\ldots10^{5}$ range (see supplementary information). With growing $\overline{k_a}$, the sensitivity band shifts slightly upwards along the K_H direction. However further increase of $\overline{k_a}$ above 10^2

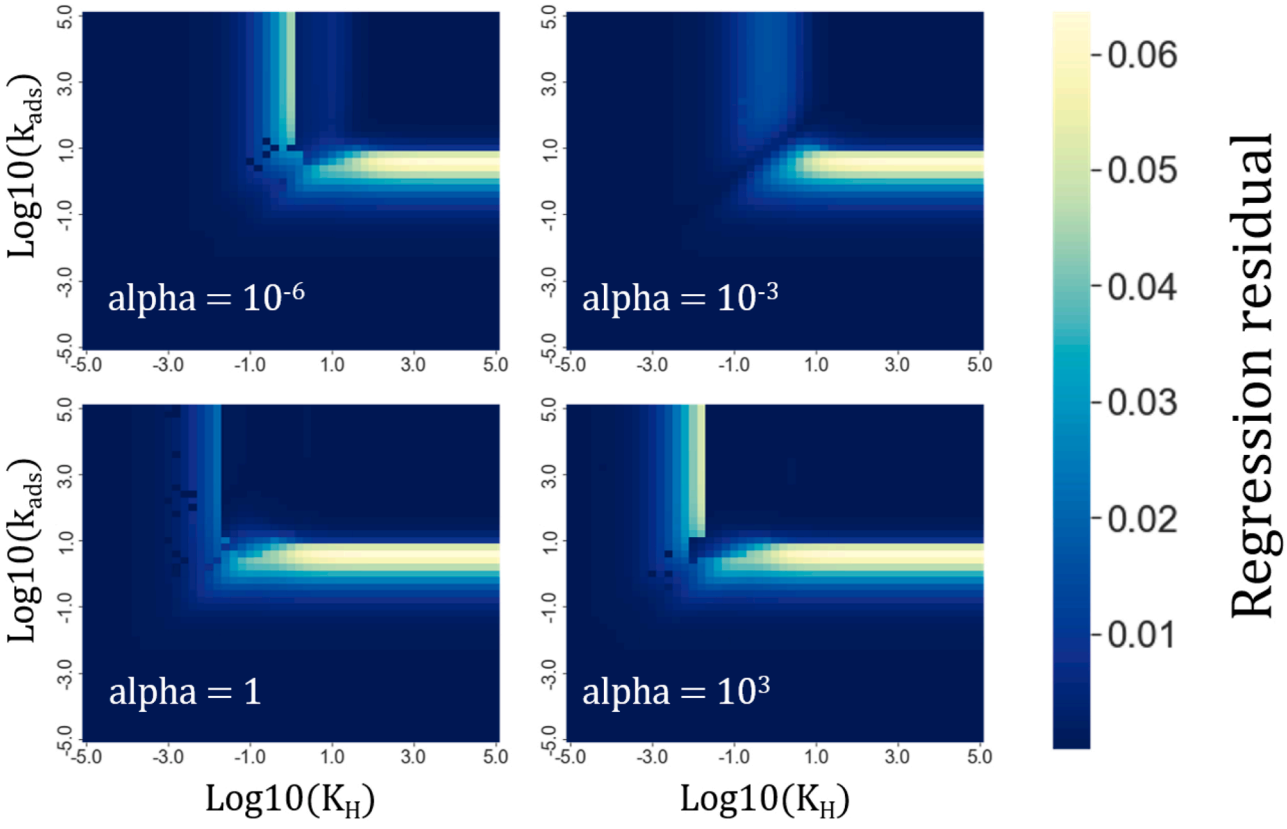

Fig. 11. Regression residual of curves simulated with dynamic adsorption model (Model 2) withing certain parametric input and regressed by Keipert model.

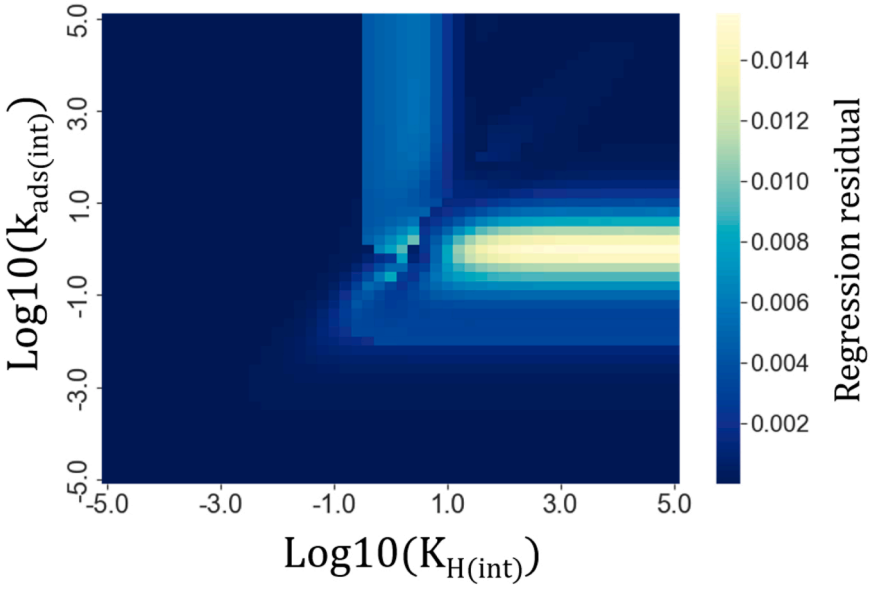

Fig. 12. Regression residual of curves simulated Model 5 and regressed by Model 2.

influences neither the sensitivity values nor the position of the band, indicating the convergence to a simpler Keipert model.

Next, we extend our analysis to a more detailed model that also explicitly captures the transport resistance at the pore entry, i.e. the surface barrier. The sensitivity of this model to the surface permeation parameter $\overline{k_{ent}}$ is evaluated at a single set of the external adsorption parameters, out of the equilibrium adsorption region ($\overline{k_a} = 10, \overline{k_d} = 10^2$). Fig. 10 depicts the sensitivity of the model response to $K_p = \overline{k_{ent}}/\overline{k_{ext}}$ and α at different values of $\overline{k_{ent}}$. Similarly to Fig. 7, two regions of low sensitivity are separated by an intense sensitivity band. In the region above the band, the rate of pore entry strongly dominates over the rate of pore exit, resulting in negligible amounts of gas exiting the microporous domain - a zone of "no escape". Conversely, the shape of the pulse-response curve in the opposite region of "no entry" is dictated only by the $\overline{k_a}$ and $\overline{k_d}$ values because the rate of the pore entry is very low. Also analogously to Figs. 7 and 9, the two arms of the sensitivity band stem from the same region with $log(\alpha) = 0$, above which the pulse-response curves are insensitive to α.

3.2. Regression analysis

In a typical experiment, prior knowledge about the operating condition window in terms of gas/zeolite interactions is rarely available: whether it is in the region of equilibrium or dynamic adsorption at the pore mouth, slow microporous diffusion or slow surface permeation etc. Some insight into the relative influence of reaction and diffusion can potentially be gained from the available complementary data or the literature in simple cases, for example, Thiele modulus can suggest whether the process operates in the diffusion-controlled or reaction-controlled space. However, comparison of relevant time-scales in other domains, besides diffusion/reactivity is not straightforward. The α parameter that reflects the time-scale ratio between the bulk and microporous diffusivities in complex models cannot be analyzed in a similar to Thiele modulus fashion, since the sensitivity portrait of these models contains several sub-domains: fast microporous diffusion at $\alpha > 1$; the sensitivity band between $\alpha = 10^{-5}$ and $\alpha > 1$; and another zone of insensitivity due to slow diffusion at $\alpha < 10^{-5}$. Based on the analysis provided in the previous section, judging the transport region only by means of $\alpha \leq 1$ or ≥ 1 would not be sufficient. It is, therefore, important to consider at what values of parameters the dynamic adsorption model (Model 2) converges to the equilibrated Keipert model. To this end, we performed multiparametric regression study in which pulse-response curves simulated with the dynamic adsorption (Model 2) model were regressed with the simpler Keipert model for various α values and different k_a and K_H values. The accumulated residual between the simulated and regressed responses was calculated and plotted along the parameters axes to elucidate convergence between the two models.

In Fig. 11, the regions of poor agreement between the simple equilibrium adsorption and the dynamic adsorption models can be observed. Each plot resembles two perpendicular lines meeting at a certain point: when $\alpha < 1$ it is the center of the plot ($log(K_H) = 0$ and $log(\overline{k_{ads}}) = 0$), and when $\alpha \geq 1$ the point shift to smaller $K_H = 10^{-2}$. Equilibrium adsorption conditions start at $\overline{k_{ads}}$ values above $10 - 100$, which is consistent with results from previous section. In the range of K_H values between 10^{-3} to 10 (depending on α values), the shapes produced by the dynamic adsorption model could not be adequately described by the equilibrium model. This information is valuable for designing statistical analysis protocols for model assessment - when using the adsorption constants from the literature or post-processed data, we can accept or discard the Keipert model based on the values of estimated $\overline{k_{ads}}$ and K_H.

Another valuable model delineation emerges when contrasting the model containing microporous diffusion as a Fickian term, corresponding to random walk diffusion mechanism, and the model additionally accounting for a microkinetic term describing stronger, presumably activated hopping mechanisms between adjacent surface sites within the pores. Simulated data were generated within a wide range of $k_{ads(int)}$ and $K_{eq(int)}$ by the more generally valid Model 5 and then regressed using a simpler, Fickian-only Model 2. As evident from Fig. 12, Model 5 model can produce unique shapes not fully captured by the (DAMP) model. More specifically, this occurs in the region of medium-high k_{ads} ($K_{eq(int)} = 0.1 - 10$) and in the region of medium-high $K_{eq(int)}$($k_{ads} = 0.01 \ldots 10$). The graph resembles Fig. 11, where the two bands of large regression residuals meet at the center of the plot. This simple virtual experiment clearly demonstrates that the shapes of the pulse-response curves encountered in a real experiment can be distinct from the ones prescribed by simple models and suggests the signs that a more detailed model must be employed for data analysis.

3.3. Influence of adsorption thermodynamics

In this section, we predict how realistic values of thermodynamic

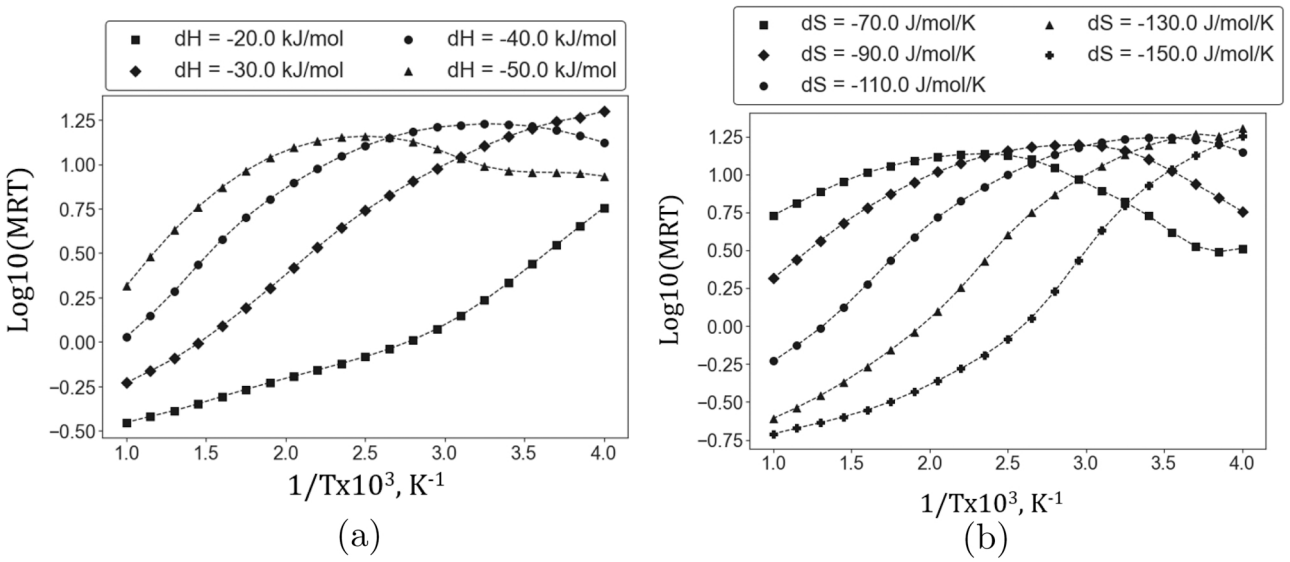

Fig. 13. Simulated by Model 5 temperature dependency of mean residence time (MRT) in the TAP reactor with variable ΔH_{ads} and ΔS_{ads}.

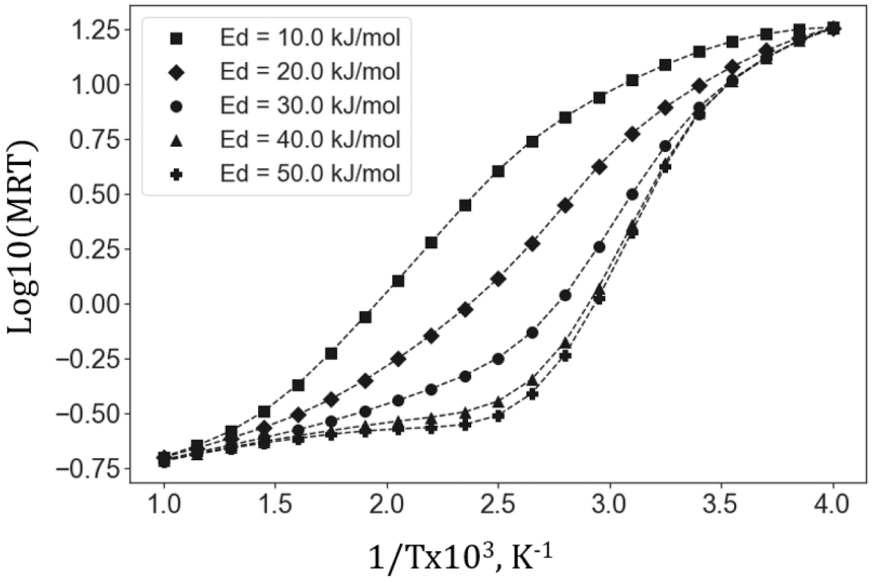

Fig. 14. Simulated by Model 5 temperature dependency of mean residence time (MRT) in the TAP reactor with variable E_{Diff}.

adsorption parameters for practical zeolites influence the shapes of the pulse-response curves. Mean residence time (MRT) was chosen as a shape descriptor, since it can be readily extracted from raw data and is commonly reported in the literature.

The k_{ads} values were prescribed using the Hertz-Knudsen equation, and thermodynamic consistency was used to estimate k_{des}. This implies that variations of adsorption thermodynamics ΔH_{ads} and ΔS_{ads} only affected the value of k_{des}, somewhat limiting the scope of our analysis. However, similar trends are expected for other possible dependencies of k_{ads} on temperature.

The observed temperature dependencies of MRT on temperature were non-monotonous and exhibited a maximum, depending on a particular combination of parameters used. Variation of ΔH_{ads} and ΔS_{ads} for both models, with and without internal adsorption, showed that the decrease of the free energy of adsorption $\Delta G_{ads} = \Delta H_{ads} - T\Delta S_{ads}$ (more negative) lowers the value of MRT peak and shifts the peak position to higher temperatures Fig. 13.

Variation of E_{diff} and D_{p0} showed that slower microporous diffusion shifts the peak of MRT temperature dependency to lower temperatures. More importantly, slow microporous diffusion curves acquire a pronounced characteristic bend in the MRT temperature dependency, which provides a novel fingerprint for distinguishing slow from fast microporous transport in experimental data Fig. 14.

It is particularly interesting to investigate the difference between the energies of adsorption on the outer surface and internal active sites in zeolites. Fig. 15 presents how the difference in adsorption enthalpies between the two types of sites affects MRT. When enthalpy of internal adsorption is less negative (weaker adsorption) or equal to enthalpy of surface adsorption, DSAMA model converges to the DAMP model. However, when the internal adsorption enthalpy is more negative (stronger adsorption), a significant difference between the MRT dependencies is observed. At moderate enthalpy difference, MRT gains an extra plateau at lower temperatures, while at higher differences even extra peaks of MRT can occur. These newly found model features will aid in experimental investigations of microporous materials with energetically different adsorption sites, which are frequently encountered in

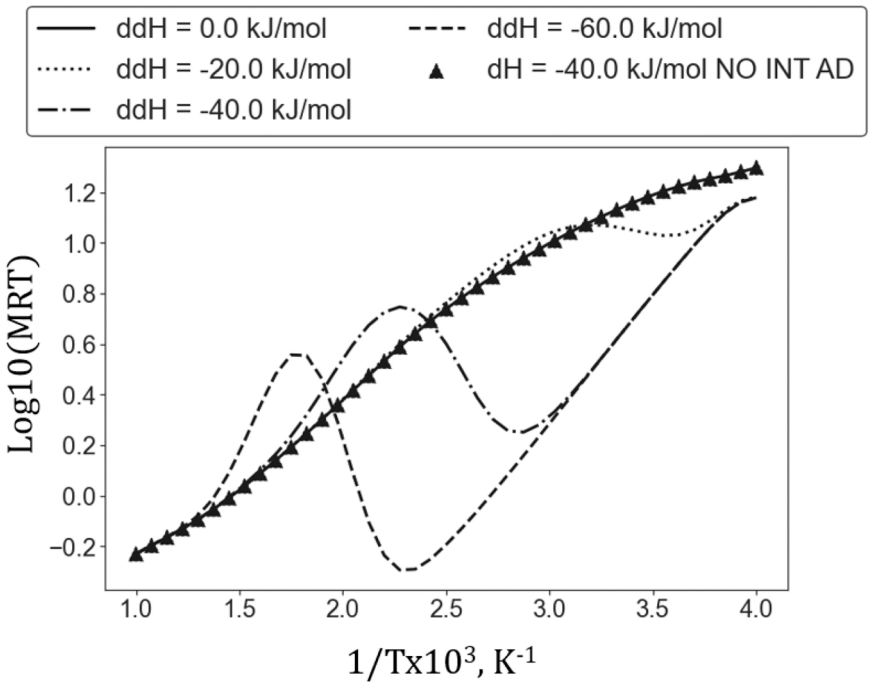

Fig. 15. Simulated temperature dependency of MRT in the TAP reactor with variable adosprtion enthalpy difference between external and interal active sites $\Delta\Delta H_{ads}$ (where $\Delta\Delta H_{ads} = \Delta H_{ads} - \Delta H_{ads(int)}$).

catalysis by zeolites.

4. Conclusions

Mathematical models of pulse-response TAP experiments were constructed that account for a multitude of processes encountered within microporous materials. Models reflecting surface barriers and decoupled intraporous adsorption and diffusivity terms were developed and studied for the first time. Rigorous sensitivity analysis delineated the parametric windows where such models converge to the same behavior. Furthermore, novel fingerprints were described that can aid in the identification of appropriate parametric domains for regression of experimental data with clear extrema in the temperature dependency of the mean residence time. Future work will focus on validating these findings with experimental TAP data conducted for well-defined zeolite materials that can exhibit target features (e.g. slow microporous diffusion, energetic difference between surface and internal active sites, etc.) Potential extensions to our analysis will also explore the use of more mathematically advanced mathematical techniques of model interrogation, such as the use of Sobolev's co-dispersion to quantify parameter correlations. Overall, we conclude that robust mathematical models are a cornerstone of any transient kinetics method and must be advanced concurrently with the development of new measurement techniques and tailored catalytic materials. Appropriate high-fidelity models can provide access to materials descriptors that were previously unavailable from macroscopic measurements.

Declaration of Competing Interest

The authors declare that they have no known competing financial interests or personal relationships that could have appeared to influence the work reported in this paper.

Acknowledgements

E.R. and U.O. acknowledge funding provided by the Research Council of Norway (contract 288331, CO2LO project). V.S. acknowledges funding provided by the Department of Chemistry at the University of Oslo (UiO). We would also like to express our gratitude to Prof. Einar Uggerud at the Department of Chemistry, UiO for many fruitful scientific discussions that contributed to this work.

CRediT authorship contribution statement

Vladyslav Shostak: Formal analysis, Writing – original draft, Methodology, Software. **Evgeniy Redekop:** Methodology, Writing – review & editing. **Unni Olsbye:** Conceptualization, Validation, Supervision, Project administration.

Appendix A. Supporting information

Supplementary data associated with this article can be found in the online version at doi:10.1016/j.cattod.2022.05.050.

Appendix A. Ratio between dimensional and dimensionless parameters

1. Variables:

$$\begin{aligned}\overline{C_A} &= \frac{\varepsilon_b AL}{N_p} C_A \\ \overline{\theta_A} &= \frac{A_S S_V}{N_p} AL(1-\varepsilon_b)\theta_A \\ \overline{C_{pA}} &= \frac{\varepsilon_p(1-\varepsilon_b)AL}{N_p} C_{pA} \\ \overline{\theta_{A(int)}} &= \frac{A_{S(int)}}{N_p} AL(1-\varepsilon_b)\theta_{A(int)}\end{aligned} \tag{36}$$

2. Scaling:

$$\tau = \frac{tD_b}{\varepsilon_b L^2}; \qquad \zeta = \frac{z}{L}; \qquad \rho = \frac{r}{R}. \tag{37}$$

3. Parameters:

$$\begin{aligned}\overline{k_a} &= \frac{L^2}{D_b}(1-\varepsilon_b)A_S S_V k_a \\ \overline{k_d} &= \frac{\varepsilon_b L^2}{D_b} k_d \\ \overline{k_{ent}} &= \frac{\varepsilon_b L^2}{D_b} k_{ent} \\ \overline{k_{ext}} &= \frac{AL^2}{D_b} k_{ext} \\ \overline{k_{a(int)}} &= \frac{A_{S(int)} R^2}{D_p} k_{a(int)} \\ \overline{k_{d(int)}} &= \frac{\varepsilon_b R^2}{D_p} k_{d(int)}\end{aligned} \tag{38}$$

4. Options

$$\begin{aligned}\alpha &= \frac{\varepsilon_b L^2}{D_b}\frac{D_p}{\varepsilon_p R^2} \\ \beta &= S_v R \\ \delta &= \frac{R}{\Delta l}\end{aligned} \tag{39}$$

References

[1] U. Olsbye, et al., Conversion of methanol to hydrocarbons: how zeolitecavity and pore size controls product selectivity, Angew. Int. Ed. 51 (24) (2012) 5810–5831, https://doi.org/10.1002/anie.201103657.
[2] D. Constales, G.S. Yablonsky, G.B. Marin, J.T. Gleaves, Multi-zone TAP-reactors theory and application: I. The global transfer matrix equation, Chem. Eng. Sci. 56 (1) (2001) 133–149, https://doi.org/10.1016/S0009-2509(00)00216.
[3] K. Jorg, D.M. Ruthven, and T.D.N., Diffusion in nanoporous materials.Wiley, 2010. ISBN: 978–3-527–31024-.
[4] K. Morgan, et al., Forty years of temporal analysis of products, Catal. Sci. Technol. 7 (12) (2017) 2416–2439, https://doi.org/10.1039/C7CY00678K.
[5] J.T. Gleaves, G. Yablonsky, X. Zheng, R. Fushimi, P.L. Mills, Temporal analysis of products (TAP)-Recent advances in technology forkinetic analysis of multi-component catalysts, J. Mol. Catal. A Chem. 315 (2) (2010) 108–134, https://doi.org/10.1016/j.molcata.2009.06.017.
[6] J.T. Gleaves, G.S. Yablonskii, P. Phanawadee, Y. Schuurmanb, APPLIED CATALYSIS TAP-2: An interrogative kinetics approach.1997.
[7] M.J. Vaezi, M.E. Kojabad, M.M. Beiragh, A.A. Babaluo, Transport Mechanism and Modeling of Microporous Zeolite Membranes, Curr. Trends Futur. Dev. Membr. Microporous Membr. Membr. React. (2019) 185–203, https://doi.org/10.1016/B978-0-12-816350-4.00008-8.
[8] H.G. Karge, J. Kärger, Application of IR spectroscopy, IRmicroscopy, and optical interference microscopy to diffusion in zeolites, Mol. Sieves Sci. Technol. 7 (2008) 135–206, https://doi.org/10.1007/3829_2008_020.
[9] J. Kärger, Diffusion measurements by NMR techniques, Adsorpt. Diffus. 7 (2008) 85–133, https://doi.org/10.1007/3829_2007_019.
[10] J. Kärger, et al., Benefit of microscopic diffusion measurement for the characterization of nanoporous materials, Chem. Eng. Technol. 32 (10) (2009) 1494–1511, https://doi.org/10.1002/CEAT.200900160.
[11] A.R. Teixeira, C.-C. Chang, T. Coogan, R. Kendall, W. Fan, P.J. Dauenhauer, Dominance of surface barriers in molecular transport through silicalite-1, J. Phys. Chem. C 117 (48) (2013) 25545–25555, https://doi.org/10.1021/jp4089595.
[12] L. Karwacki, et al., Morphology-dependent zeolite intergrowth structures leading to distinct internal and outer-surface molecular diffusion barriers, Nat. Mater. 8 (12) (2009) 959–965, https://doi.org/10.1038/nmat2530.
[13] P. Cnudde, et al., Experimental and theoretical evidence for the promotional effect of acid sites on the diffusion of alkenes through small-pore zeolites, Angew. Chem. - Int. Ed. (2021) 10016–10022, https://doi.org/10.1002/anie.202017025.

[14] J.A. Boscoboinik, et al., Modeling zeolites with metal-supported two-dimensional aluminosilicate films, Angew. Chem. Int. Ed. 51 (24) (2012) 6005–6008, https://doi.org/10.1002/anie.201201319.
[15] N. Hansen, F.J. Keil, Multiscale modeling of reaction and diffusion in zeolites: from the molecular level to the reactor, Soft Mater. 10 (1–3) (2012) 179–201, https://doi.org/10.1080/1539445X.2011.599708.
[16] J.-M. Schweitzer, et al., Multiscale modeling as a tool for the prediction of catalytic performances: the case of n-heptane hydroconversion in a large-pore zeolite, ACS Catal. 12 (2) (2022) 1068–1081, https://doi.org/10.1021/ACSCATAL.1C04707.
[17] F.J. Keil, Kinetics of chemical reactions. decoding complexity. by guy marin and gregory S. Yablonsky, Angew. Chem. Int. Ed. 51 (29) (2012) 7080–7081, https://doi.org/10.1002/ANIE.201203510.
[18] T.A. Nijhuis et al., Measurement and modeling of the transient adsorption, desorption and diffusion processes in microporous materials.
[19] S.V. Nayak, M. Morali, P.A. Ramachandran, M.P. Dudukovic, Transport and sorption studies in beta and USY zeolites via temporal analysis of products (TAP), J. Catal. 266 (2) (2009) 169–181, https://doi.org/10.1016/j.jcat.2009.06.008.
[20] Y. SCHUURMAN, Assessment of kinetic modeling procedures of TAP experiments, Catal. Today 121 (3–4) (2007) 187–196, https://doi.org/10.1016/j.cattod.2006.06.046.
[21] R. Batchu, et al., Ethanol dehydration pathways in H-ZSM-5: insights from temporal analysis of products, Catal. Today 355 (April) (2020) 822–831, https://doi.org/10.1016/j.cattod.2019.04.018.
[22] E. Gutierrez Acebo, Impact of the topology of the zeolite structureon the mechanism and selectivity of ethylcyclohexane bifunctional isomerization: experiments, ab initio calculations and multi-scale kinetic modelling. Accessed: Jan. 31, 2022. [Online]. Available: ⟨https://tel.archives-ouvertes.fr/tel-02373422⟩.
[23] Y. Chapellière, C. Daniel, A. Tuel, D. Farrusseng, Y. Schuurman, Kinetics of n-hexane cracking over mesoporous hy zeolites based on catalyst descriptors, Catalysts 11 (6) (2021), https://doi.org/10.3390/catal11060652.
[24] E.A. Redekop, A. Lazzarini, S. Bordiga, U. Olsbye, A temporal analysis of products (TAP) study of C2-C4 alkene reactions with a well-defined pool of methylating species on ZSM-22 zeolite, J. Catal. 385 (2020) 300–312, https://doi.org/10.1016/j.jcat.2020.03.020.
[25] T. Omojola, A.J. Logsdail, A.C. Van Veen, S.A.F. Nastase, A quantitative multiscale perspective on primary olefin formation from methanol, Phys. Chem. Chem. Phys. 23 (38) (2021) 21437–21469, https://doi.org/10.1039/D1CP02551A.
[26] O. Dewaele, V.L. Geers, G.F. Froment, G.B. Marin, Theconversion of methanol to olefins: a transient kinetic study, Chem. Eng. Sci. 54 (20) (1999) 4385–4395, https://doi.org/10.1016/S0009-2509(98)00533-8.
[27] O.P. Keipert and M. Baerns al', Determination of the intracrystalline diffusion coefficients of alkanes in H-ZSM-5 zeolite by a transient technique using the temporal-analysis-of-products (TAP) reactor.1998.
[28] A.H.J. Colaris, J.H.B.J. Hoebink, M.H.J.M. de Croon, J.C. Schouten, Intrapellet diffusivities from TAP pulse responses via moment-based analysis, AIChE J. 48 (11) (2002) 2587–2596, https://doi.org/10.1002/aic.690481117.
[29] S.O. Shekhtman, G.S. Yablonsky, S. Chen, J.T. Gleaves, Thin-zone TAP-reactor - theory and application, Chem. Eng. Sci. 54 (20) (1999) 4371–4378, https://doi.org/10.1016/S0009-2509(98)00534-X.
[30] P. Phanawadee, S.O. Shekhtman, C. Jarungmanorom, G.S. Yablonsky, J.T. Gleaves, Uniformity in a thin-zone multi-pulse TAP experiment: numerical analysis, Chem. Eng. Sci. 58 (11) (. 2003) 2215–2227, https://doi.org/10.1016/S0009-2509(03)00080-0.
[31] S.O. Shekhtman, G.S. Yablonsky, J.T. Gleaves, R.R. Fushimi, Thin-zone TAP reactor as a basis of 'state-by-state transient screening, Chem. Eng. Sci. 59 (22–23) (2004) 5493–5500, https://doi.org/10.1016/J.CES.2004.09.015.
[32] M.I. Temkin, The kinetics of some industrial heterogeneous catalytic reactions, Adv. Catal. 28 (C) (1979) 173–291, https://doi.org/10.1016/S0360-0564(08)60135-2.
[33] S.O. Shekhtman, G.S. Yablonsky, Thin-zone TAP reactor versusdifferential PFR: analysis of concentration nonuniformity for gas-solid systems, Ind. Eng. Chem. Res. 44 (16) (2005) 6518–6522, https://doi.org/10.1021/IE010195Z.
[34] J.G. Choi, D.D. Do, H.D. Do, Surface diffusion of adsorbedmolecules in porous media: monolayer, multilayer, and capillary condensation regimes, Ind. Eng. Chem. Res. 40 (19) (2001) 4005–4031, https://doi.org/10.1021/IE010195Z.
[35] J. Kärger, Single-file diffusion in zeolites, Mol. Sieves Sci. Technol. 7 (2008) 329–366, https://doi.org/10.1007/3829_2007_018.
[36] J.M. Simon, J.P. Bellat, S. Vasenkov, J. Kärger, Sticking probability on zeolites, J. Phys. Chem. B 109 (28) (2005) 13523–13528, https://doi.org/10.1021/JP0511606.
[37] B.A. De Moor, M.F. Reyniers, O.C. Gobin, J.A. Lercher, G.B. Marin, Adsorption of C2-C8 n-alkanes in zeolites, J. Phys. Chem. C 115 (4) (2011) 1204–1219, https://doi.org/10.1021/JP106536M.
[38] B.A. De Moor, M.F. Reyniers, G.B. Marin, Physisorption and chemisorption of alkanes and alkenes in H-FAU: a combined ab initio-statistical thermodynamics study, Phys. Chem. Chem. Phys. 11 (16) (2009) 2939–2958, https://doi.org/10.1039/B819435C.
[39] G.E.B. Archer, A. Saltelli, I.M. Sobol, Sensitivity measures, anova-like techniques and the use of bootstrap, J. Stat. Comput. Simul. 58 (2) (1997) 99–120, https://doi.org/10.1080/00949659708811825.
[40] M.D. Morris, Factorial sampling plans for preliminary computational experiments, Technometrics 33 (2) (1991) 161–174, https://doi.org/10.1080/00401706.1991.10484804.
[41] I.M. Sobol', S. Kucherenko, Derivative based global sensitivity measures, Procedia Soc. Behav. Sci. 2 (6) (2010) 7745–7746, https://doi.org/10.1016/J.SBSPRO.2010.05.208.
[42] A. Kiparissides, S.S. Kucherenko, A. Mantalaris, E.N. Pistikopoulos, Global sensitivity analysis challenges in biological systems modeling, Ind. Eng. Chem. Res. 48 (15) (2009) 7168–7180, https://doi.org/10.1021/IE900139X.